An Infrared Study of OCS Binding and Size-selective Reactivity with Gold Clusters, Au_n^+(n = 1-10)

*Alice E. Green,[1] Sascha Schaller,[2] Gabriele Meitzyte,[1] Benjamin J. Rhodes,[1] Sean P. Kealy,[1] Alexander S. Gentleman,[1] Wieland Schöllkopf,[2] André Fielicke,[2] Stuart R. Mackenzie[1]**

[1] Department of Chemistry, University of Oxford, Physical and Theoretical Chemistry Laboratory, South Parks Road, Oxford, United Kingdom, OX1 3QZ

[2] Fritz-Haber-Institut der Max-Planck-Gesellschaft, Faradayweg 4-6, 14195 Berlin, Germany

[3] Institut für Optik und Atomare Physik, Technische Universität Berlin, Hardenbergstraße 36, 10623 Berlin

Supporting Information

Table of Contents

A. Further Experimental Data

In addition to the complexes with gold clusters presented in the main manuscript we attempted to generate similar clusters of OCS with Rh_n^+ and Pt_n^+. In both cases, however, OCS reacts with the clusters to generate sulfides, even under cooled cluster source conditions.

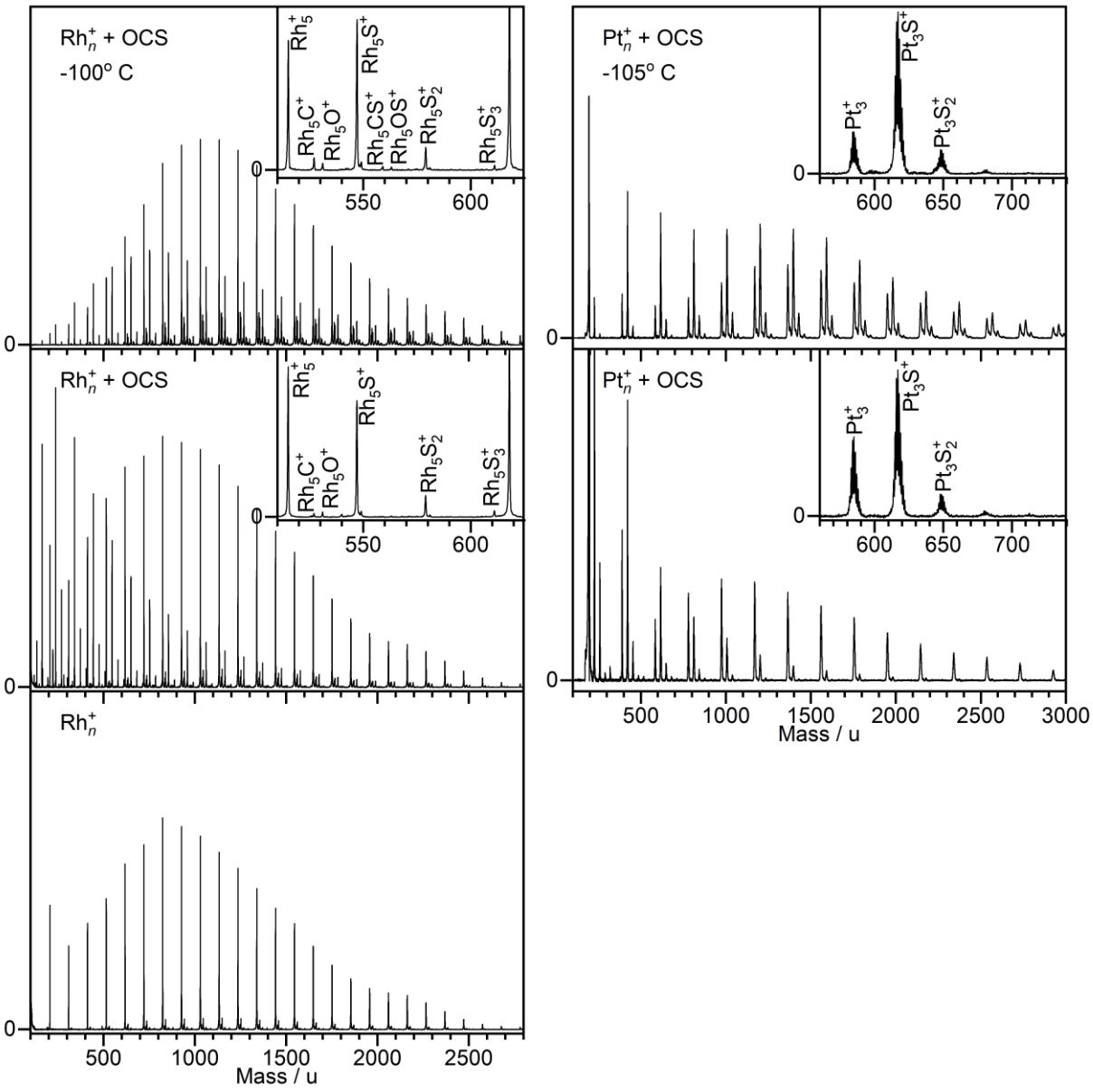

Figure S1: Time of flight mass spectra obtained following laser ablation: a) rhodium, and b) platinum targets in the presence of a carrier gas of helium and reaction gas of OCS with the source both at room temperature and cooled to -100°C. No evidence of $Rh_n(OCS)^+$ or $Pt_n(OCS)^+$ clusters was observed.

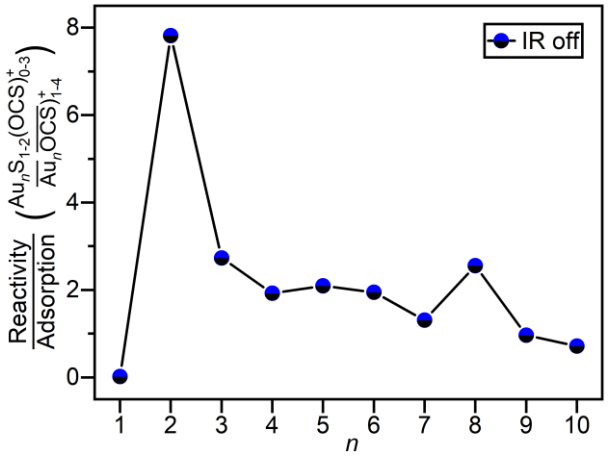

Figure S2: Ratio of sulfide-containing complexes to pure molecularly-bound clusters as a measure of relative Au_n^+ + OCS reactivity. Determined from the time of flight spectrum as integrated areas of each $Au_nS_x(OCS)_m^+$ species.

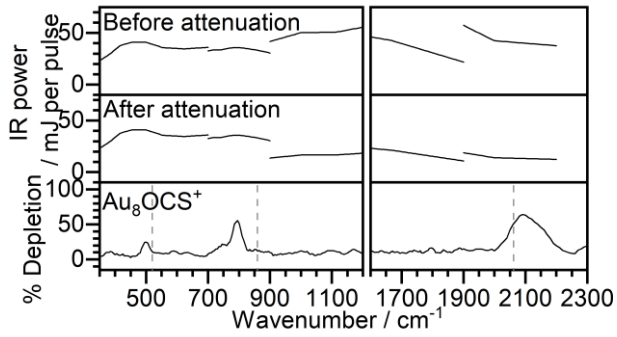

Figure S3: Free electron laser power spectrum measured close to the FEL output, alongside the IR-MPD spectrum of $Au_8(OCS)^+$.

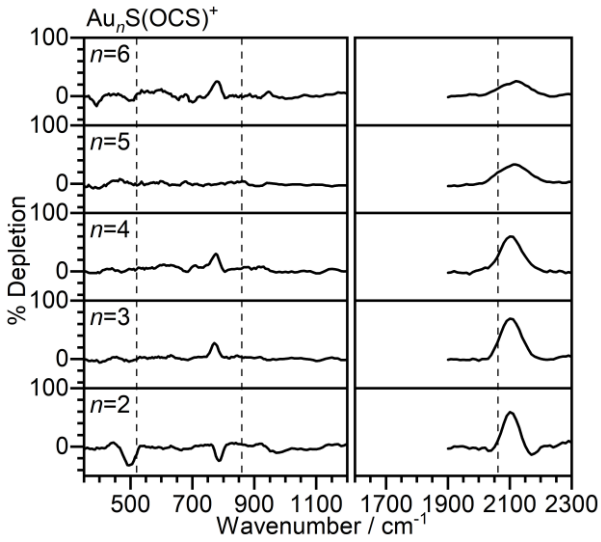

Figure S4: IR-MPD spectra of $Au_nS(OCS)^+$ (n = 2-6) clusters illustrating (with the exception of n = 5) vibrational bands characteristic of molecularly-adsorbed OCS. The dashed lines indicate the wavenumbers of the bend (520 cm^{-1}), C=S stretch (859 cm^{-1}), and C=O stretch (2062 cm^{-1}) in free OCS.[1] The 1600-1900 cm^{-1} region is unavailable for these clusters. Dips in the depletion spectra reflect dissociation into these mass channels from larger species.

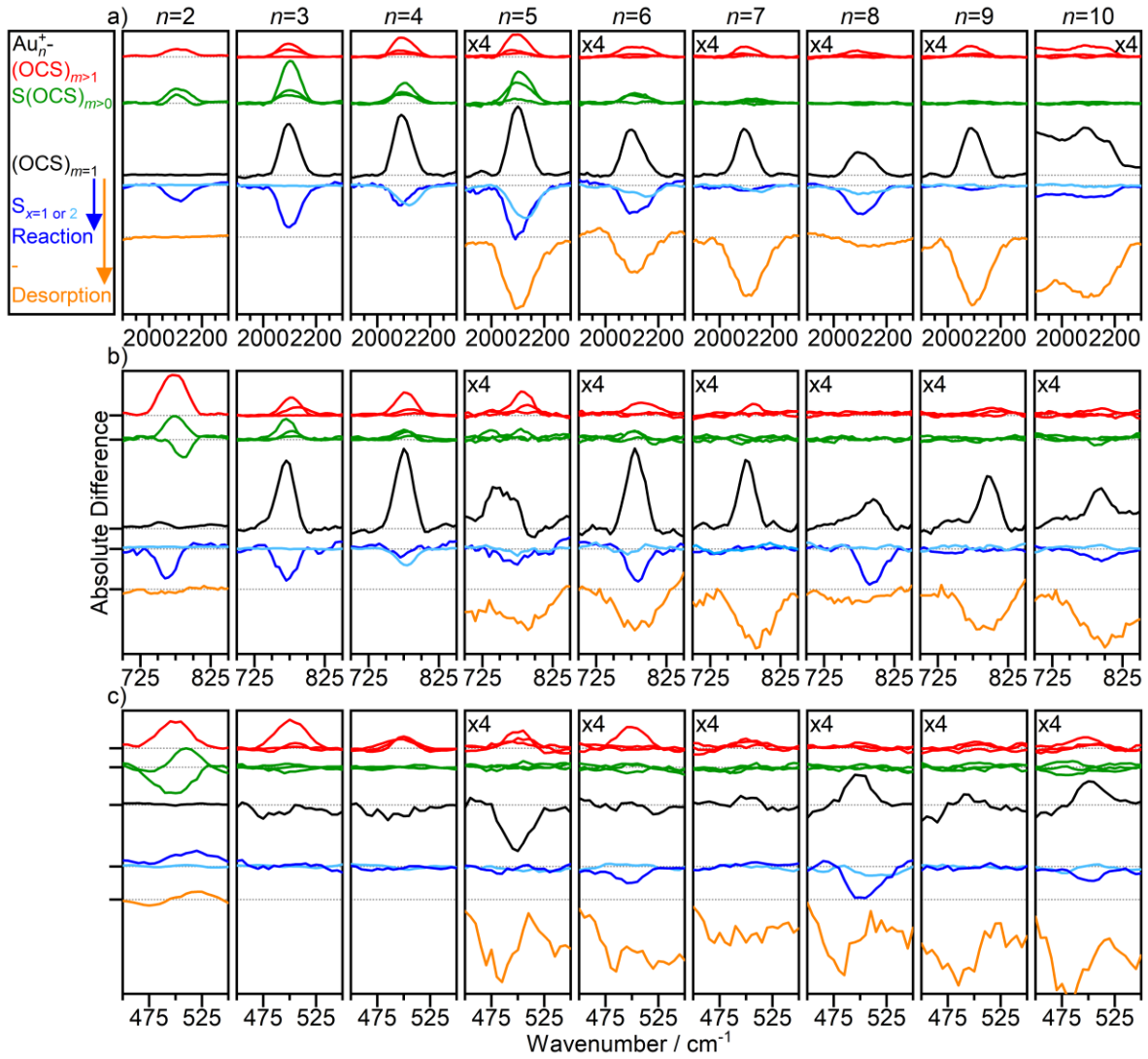

Figure S5: IR-MPD spectra of $Au_nS_x(OCS)_m^+$ (n = 2-10, m = 0-4, x = 0-2) clusters plotted as absolute difference (infrared on - infrared off) in the region of a) the C=O stretch (1900-2300 cm^{-1}), b) the C=S stretch (700-850 cm^{-1}), and c) the OCS bend (450-550 cm^{-1}).

B. Computational Details

To support assignment and interpretation of the experimental IR-MPD spectra, density functional theory and harmonic vibrational frequency calculations were performed using the UB3P86,[2] hybrid density functional coupled with the SDD,[3] basis set using the Gaussian09 suite of programs.[4] This basis set allows for 60 core electrons of Au to be treated with a quasirelativistic pseudopotential. The Au_n^+, and subsequently, $Au_n(OCS)^+$ structure search was performed using a large range of chemically intuitive starting structures, in addition to the stochastic KICK algorithm developed by Addicoat and Metha.[5] The search for the Au_n^+ geometries was supported by ion mobility measurements.[6] Calculations were repeated using the TPSS-Def2TZVP,[7-9] and TPSS-Def2TZVP with Grimme D3 and Grimme D3(BJ) dispersion parameters,[10-11] to test any functional dependence.

All structures shown within the paper represent singlet (odd *n*) or doublet (even *n*) spin states. All other spin states were found to lie at least 1.2 eV higher in energy, for each cluster size, *n*, and are therefore not expected to contribute. For example, 1.97 eV higher for quartet $Au_8^+(OCS)$.

To aid comparison with experiment, calculated frequencies have been scaled by a factor of 1.039 to match the known frequencies of the C=S stretch in free OCS.[1] Scaling to other OCS vibrations makes minimal difference.

Anharmonic frequency calculations were performed and, in a similar way, calculated frequencies have been scaled by a corresponding new factor of 1.061 to match the known frequencies of the C=S stretch in free OCS.

For the potential energy profiles, connections between minima and transition states were verified using Intrinsic Reaction Coordinate (IRC) calculations.

The calculated energies of each structure are given relative to the lowest energy molecularly-bound structure, inclusive of zero-point energy. However, energies in the potential energy profiles are given relative to the Au_n^+ + OCS asymptote.

The intensity of simulated spectra are plotted as the molar absorption coefficient, ε, $dm^3mol^{-1}cm^{-1}$ (=1000 $cm^2\ mol^{-1}$), from a linear absorbance as in the Beer-lambert law:

$$\varepsilon = \frac{1}{cd} log_{10} \left[\frac{I_0(\tilde{\nu})}{I(\tilde{\nu})}\right]$$

The intensity of the transition is measured as the integrated absorption, I_{lin} (1000 cm mol^{-1}) - the area under the entire absorption band.

$$I_{lin} = \int \varepsilon \, d\tilde{\nu} = \int \frac{1}{cd} log_{10} \left[\frac{I_0(\tilde{\nu})}{I(\tilde{\nu})}\right] d\tilde{\nu}$$

In IR spectroscopy the unit of km mol^{-1} (=1000 m mol^{-1}) is also used as a measure of integrated intensity (I_{nap}) of an absorbance but based on natural logarithms, the naperian absorbance.

$$I_{nap} = \int \frac{1}{cd} \, ln \left[\frac{I_0(\tilde{\nu})}{I(\tilde{\nu})}\right] d\tilde{\nu}$$

$$I_{nap} = \int \frac{\ln(10)}{cd} \, log_{10} \left[\frac{I_0(\tilde{\nu})}{I(\tilde{\nu})}\right] d\tilde{\nu}$$

$$I_{nap}(1000 \; m \; mol^{-1}) = \int \frac{\ln(10)}{100} \, \varepsilon(1000 \; cm^2 \; mol^{-1}) \, d\tilde{\nu}(cm^{-1})$$

We can convert between the two areas simply by the factor:

$$I_{nap}(1000 \; m \; mol^{-1}) = \frac{\ln(10)}{100} I_{lin}(1000 \; cm \; mol^{-1})$$

(as implemented as default by the GaussView software,[12])

All simulated spectra have been convoluted with a Lorenztian line function with area I_{lin} and FWHM of 20 cm^{-1} for ease of comparison with experimental data.

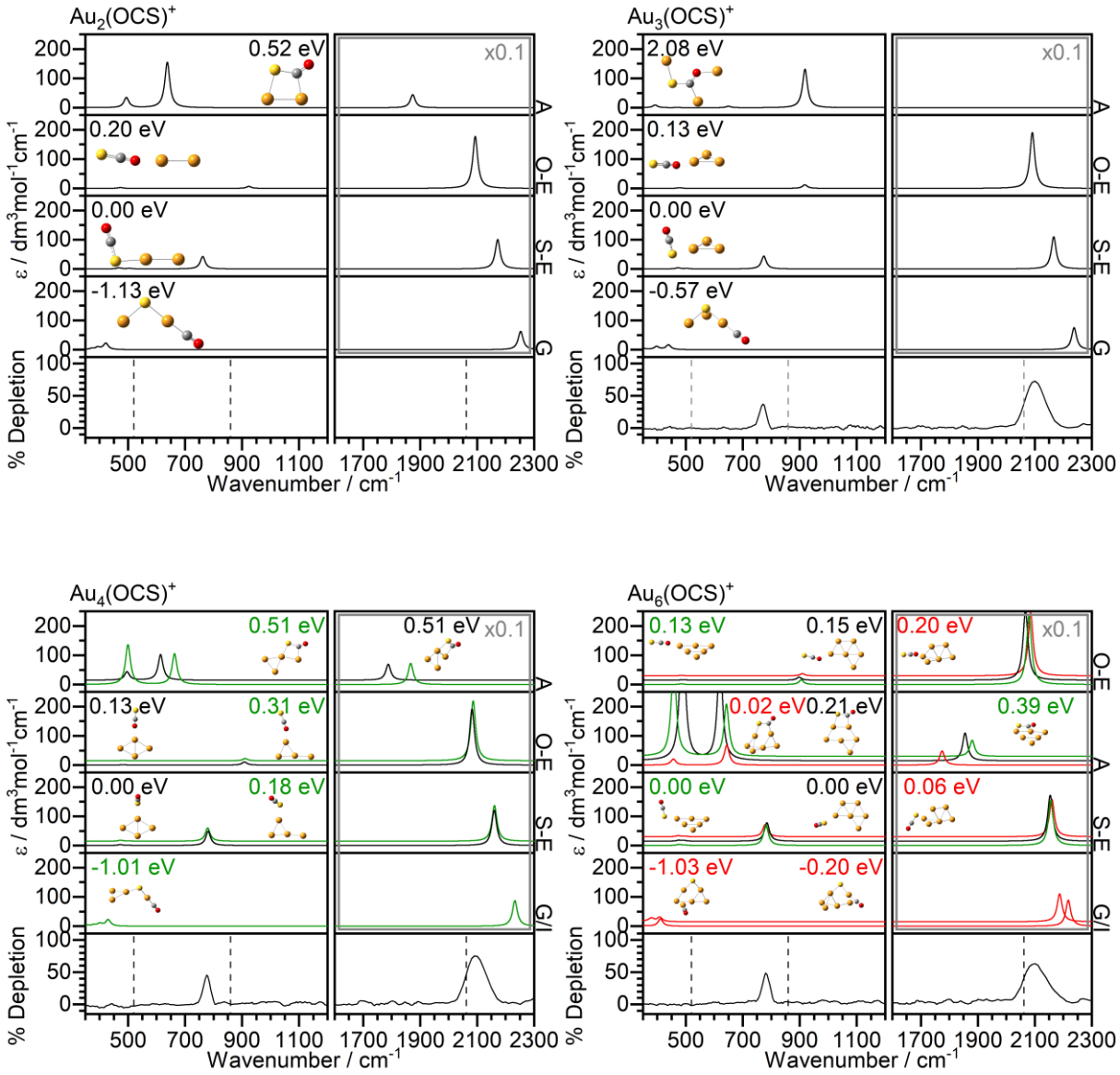

Figure S6: Comparison of the IR-MPD spectra of $Au_n(OCS)^+$ (n = 2-4, 6) with simulated IR spectra for energetically low-lying isomers, all with a singlet or doublet spin state. No spectrum could be obtained for the n = 2 cluster. n = 5 is displayed in Figure S8. All energies are relative to the lowest molecularly-bound structure and are zero-point corrected. G = global minimum inserted, I = inserted, S-E = S-bound entrance channel, O-E = O-bound entrance channel and A = activated species. Black indicates the lowest energy bare Au_n^+ structure as the base structure, green and red are base structures of slightly higher lying isomers for the bare cluster but potentially lower in energy at a different point on the potential energy surface.

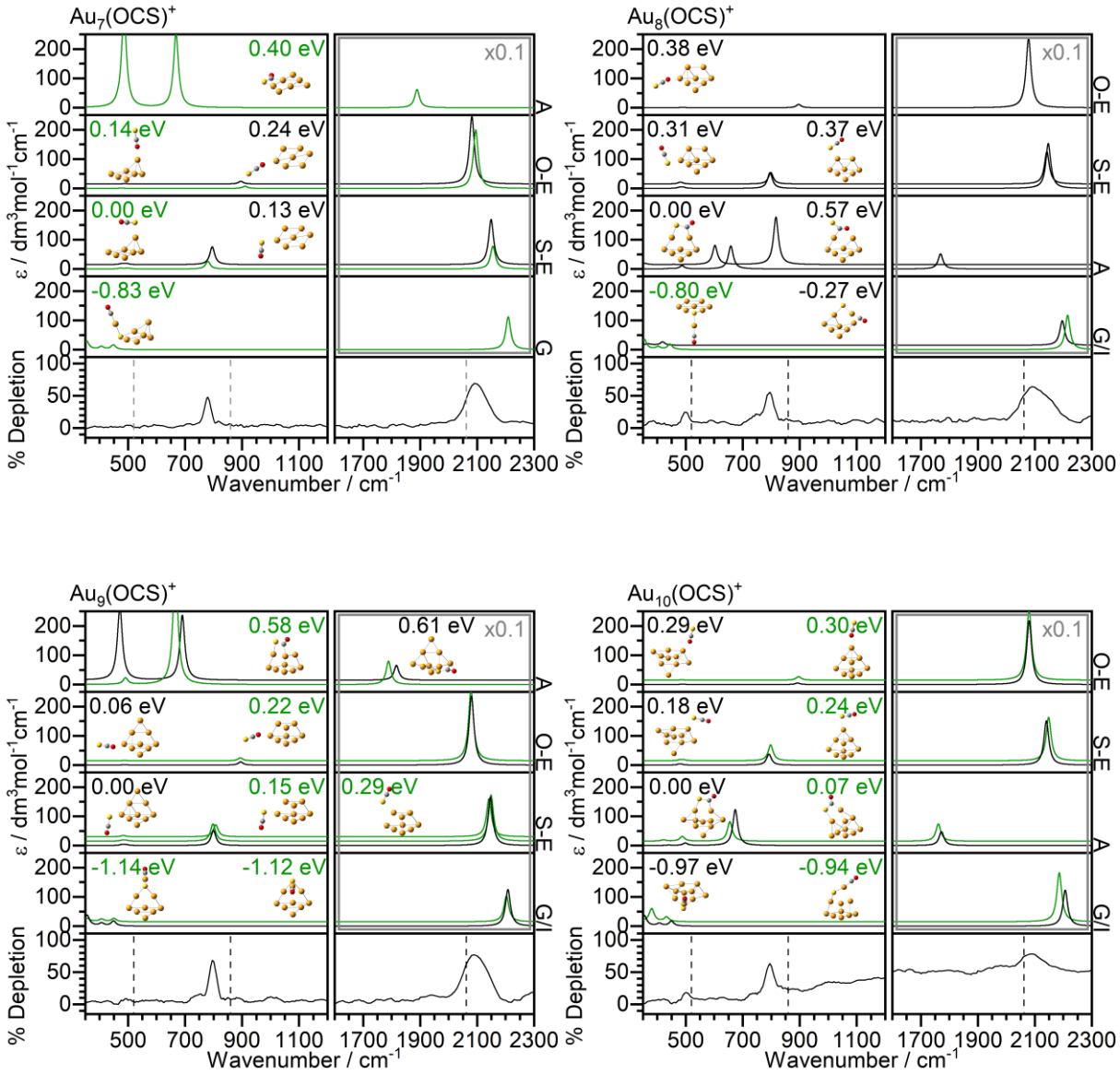

Figure S7: Comparison of the IR-MPD spectra of $Au_n(OCS)^+$ (n = 7-10) with simulated IR spectra for energetically low-lying isomers, all with a singlet or doublet spin state. All energies are relative to the lowest molecularly-bound structure and are zero-point corrected. G = global minimum inserted, I = inserted, S-E = S-bound entrance channel, O-E = O-bound entrance channel and A = activated species. Black indicates the lowest energy bare Au_n^+ structure as the base structure, green are base structures of slightly higher lying isomers for the bare cluster but potentially lower in energy at a different point on the potential energy surface.

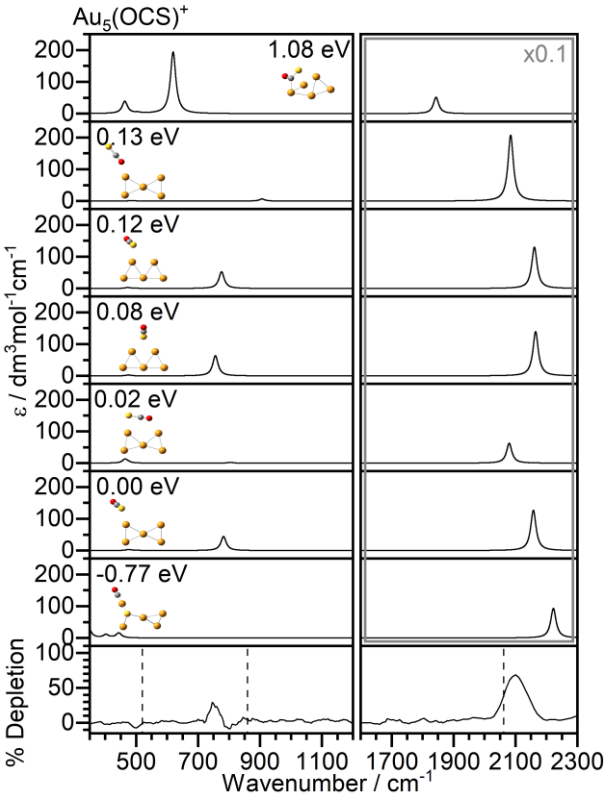

Figure S8: Comparison of the IR-MPD spectrum of $Au_5(OCS)^+$ with simulated IR spectra for energetically low-lying isomers, all with a singlet spin state. All energies are relative to the lowest molecularly-bound structure and are zero-point corrected. The flexibility of n = 5 leads to more possible binding sites.

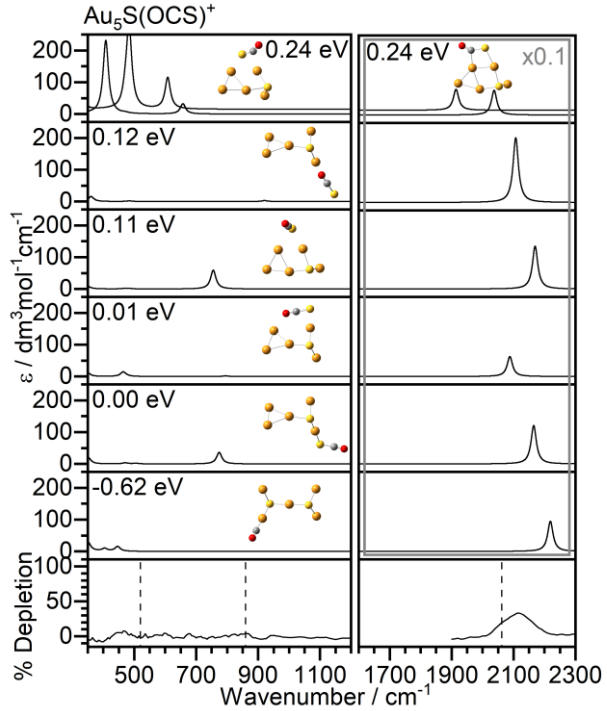

Figure S9: Comparison of the IR-MPD spectrum of $Au_5S(OCS)^+$ with simulated IR spectra for energetically low-lying isomers, all with a singlet spin state. All energies are relative to the lowest molecularly-bound structure and are zero-point corrected.

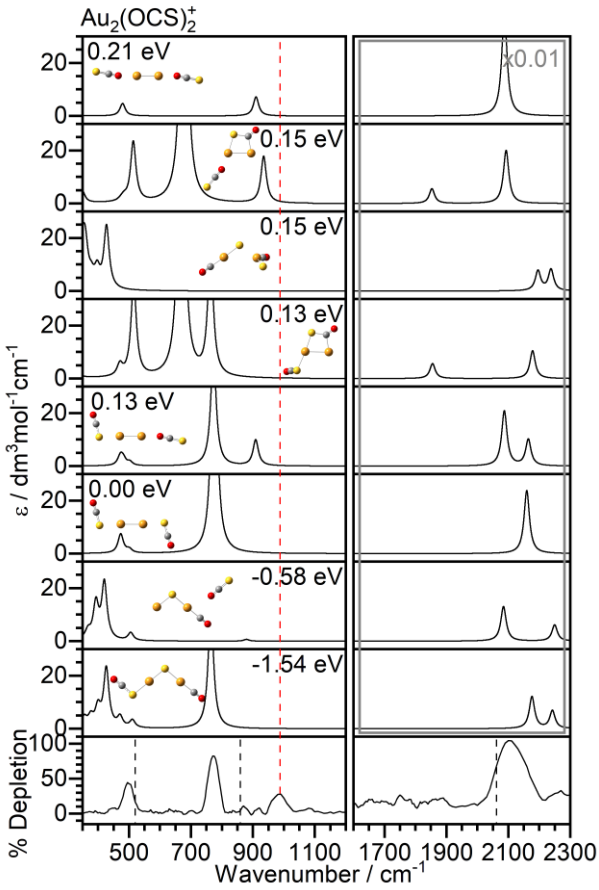

Figure S10: Comparison of the IR-MPD spectrum of $Au_2(OCS)_2^+$ with simulated IR spectra for energetically low-lying isomers, all with a doublet spin state. All energies are relative to the lowest molecularly-bound structure and are zero-point corrected. The red dotted line indicates the position of the band at 1000 cm^{-1} which cannot be explained by any of the simulated bands here.

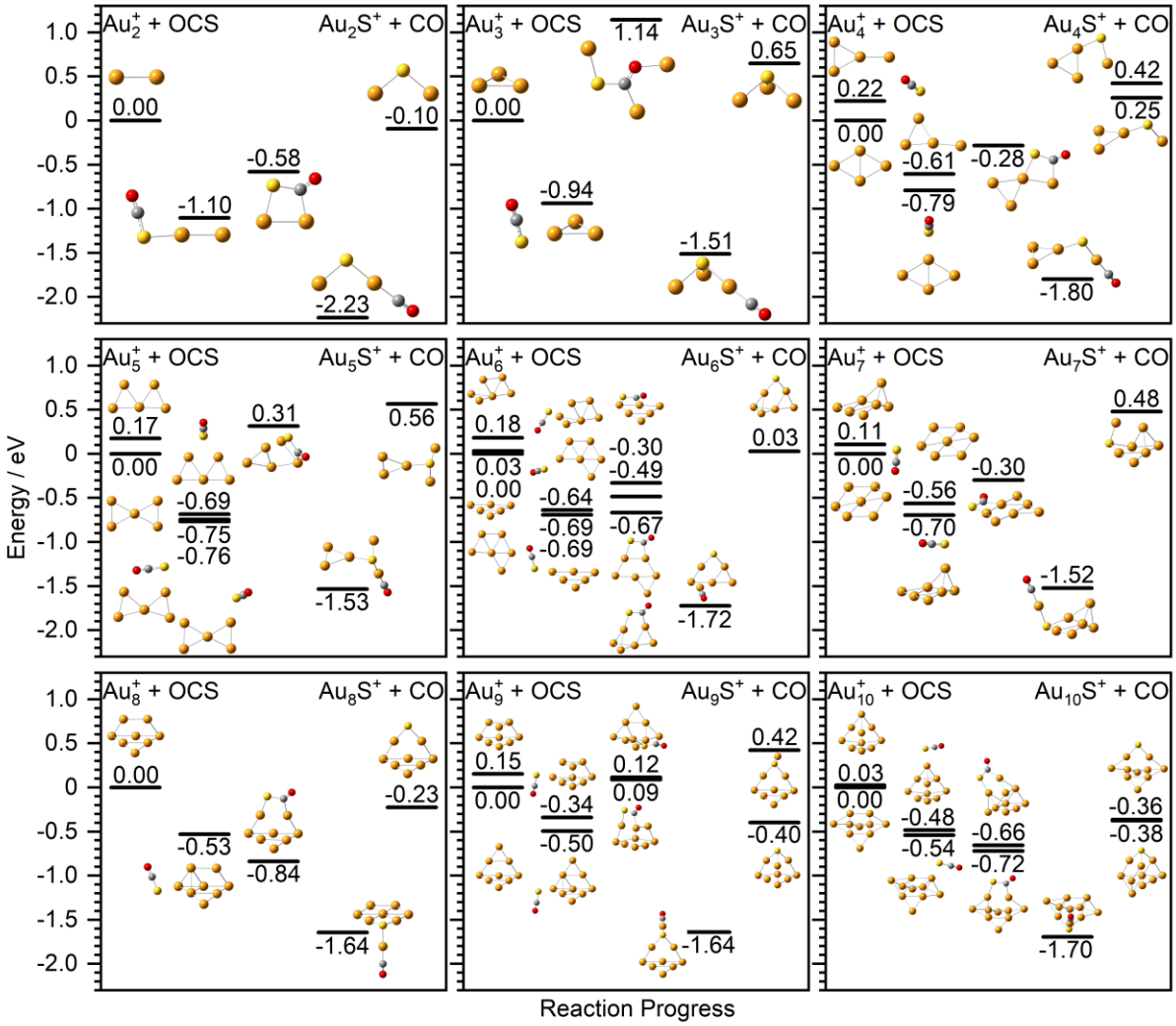

Figure S11: The minima on the potential energy surfaces of cluster sizes n = 2-10 relative to the Au_n^+ + OCS asymptote, as given in Figure 11 in the main manuscript. All energies are zero-point energy corrected. Cluster geometries and some other relevant isomers are also given here.

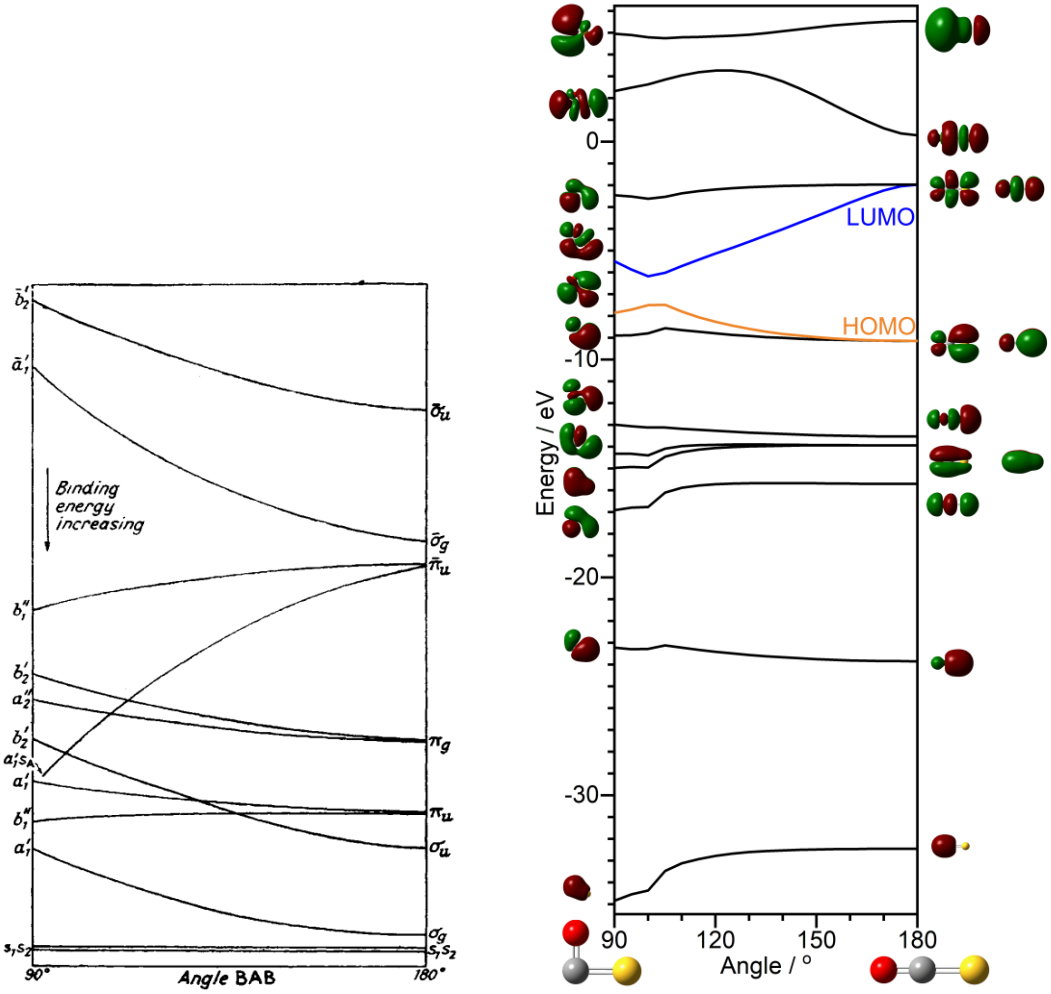

Figure S12: The Walsh diagram of AB_2 and ABC molecules taken from Walsh and coworkers,[13] reproduced with permission from the Royal Society of Chemistry and the orbital energies from single point DFT calculations of neutral OCS at 5° angle steps, keeping bond lengths constant.

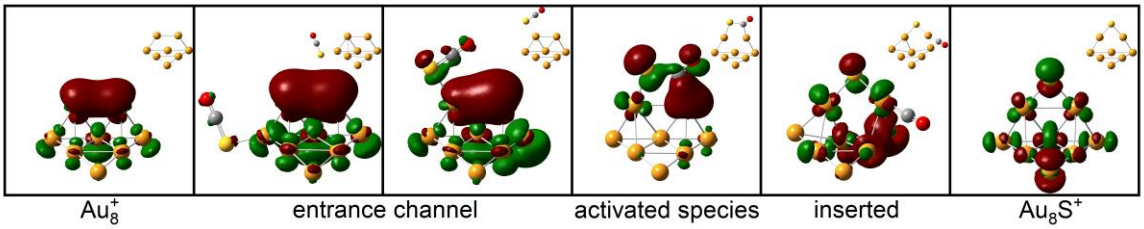

Figure S13: Molecular orbital representation of the unpaired electron along the potential energy surface of $Au_8(OCS)^+$ in Figure 10a. It shows the movement from being localised on the Au_8^+ cluster in the electrostatically-bound entrance channel species (HOMO molecular orbitals on OCS),

to donation into the antibonding LUMO of OCS in the activated species, which in turn leads to dissociation.

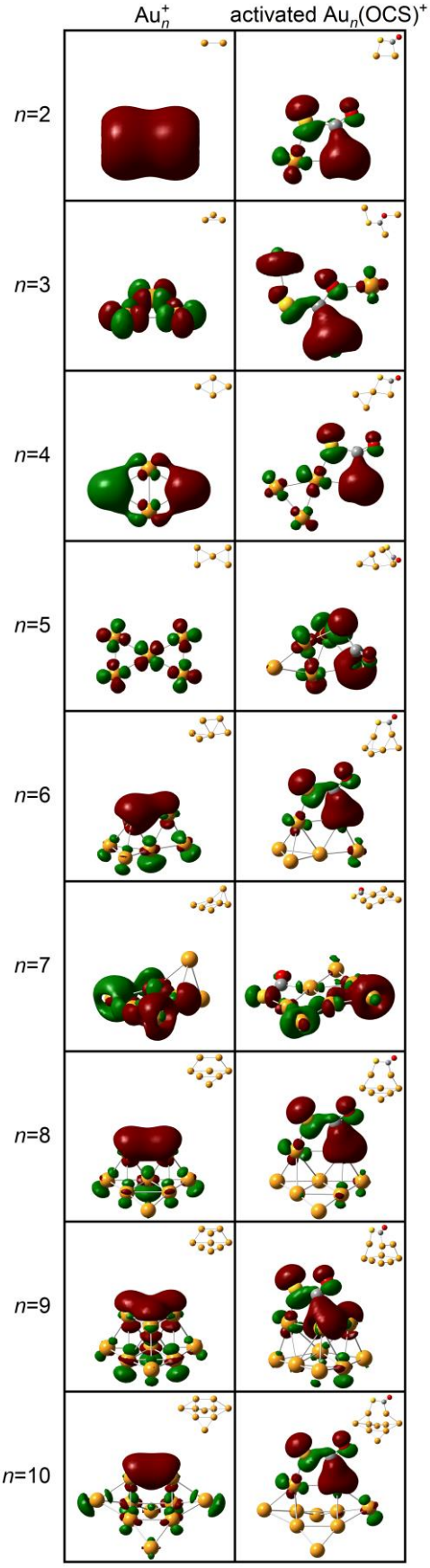

Figure S14: Molecular orbital representation of the HOMO orbital of the lowest energy activated $Au_n(OCS)^+$ species (n = 2-10) and its corresponding bare gold cluster. The HOMO is doubly occupied for odd sized clusters and singly occupied for even sized clusters.

C. References

1. Shimanouchi, T., *Tables of Molecular Vibrational Frequencies Consolidated Volume I*. Nat. Stand. Ref. Data Ser., Nat. Bur. Stand.: Wahington, D. C., 1972; Vol. 1.

2. Perdew, J. P., Density-functional approximation for the correlation energy of the inhomogeneous electron gas. *Phys Rev B* **1986,** *33* (12), 8822-8824.

3. Andrae, D.; Häußermann, U.; Dolg, M.; Stoll, H.; Preuß, H., Energy-Adjusted Ab Initio Pseudopotentials for the Second and Third Row Transition Elements. *Theor Chim Acta* **1990,** *77*, 123-141.

4. Frisch, M. J.; Trucks, G. W.; Schlegel, H. B.; Scuseria, G. E.; Robb, M. A.; Cheeseman, J. R.; Scalmani, G.; Barone, V.; Mennucci, B.; Petersson, G. A., *et al. Gaussian 09, Revision D.01*, Gaussian, Inc.: Wallingford CT, 2013.

5. Addicoat, M. A.; Metha, G. F., Kick: constraining a stochastic search procedure with molecular fragments. *J Comput Chem* **2009,** *30*, 57-64.

6. Gilb, S.; Weis, P.; Furche, F.; Ahlrichs, R.; Kappes, M. M., Structures of small gold cluster cations (Aun+, n<14): Ion mobility measurements versus density functional calculations. *J Chem Phys* **2002,** *116*, 4094-4101.

7. Perdew, J. P.; Tao, J.; Staroverov, V. N.; Scuseria, G. E., Meta-generalized gradient approximation: explanation of a realistic nonempirical density functional. *J Chem Phys* **2004,** *120* (15), 6898-911.

8. Weigend, F.; Ahlrichs, R., Balanced basis sets of split valence, triple zeta valence and quadruple zeta valence quality for H to Rn: Design and assessment of accuracy. *Phys Chem Chem Phys* **2005,** *7* (18), 3297-305.

9. Weigend, F., Accurate Coulomb-fitting basis sets for H to Rn. *Phys Chem Chem Phys* **2006,** *8*, 1057-65.

10. Grimme, S.; Antony, J.; Ehrlich, S.; Krieg, H., A consistent and accurate ab initio parametrization of density functional dispersion correction (DFT-D) for the 94 elements H-Pu. *J Chem Phys* **2010,** *132*, 154104.

11. Grimme, S.; Ehrlich, S.; Goerigk, L., Effect of the damping function in dispersion corrected density functional theory. *J Comput Chem* **2011,** *32* (7), 1456-65.

12. Dennington, R.; Keith, T. A.; Millam, J. M. *GaussView, Version 5*, Semichem Inc.: Shawnee Mission KS, 2009.

13. Walsh, A. D., The Electronic Orbitals, Shapes, and Spectra of Polyatomic Molecules . Part II. Non-Hydride AB2 and BAC Molecules. *J Chem Soc* **1953**, 2266-2288.